PROCEEDINGS A

rspa.royalsocietypublishing.org

Research

Article submitted to journal

Subject Areas:
Analogue Gravity, Nonlinear Optics, Ultrafast Optics

Keywords:
Hawking Radiation, Optical Fibers, Resonant Radiation

Author for correspondence:
Jack Petty
e-mail: jp221@st-andrews.ac.uk

THE ROYAL SOCIETY
PUBLISHING

Optical Analogue Gravity Physics - Resonant Radiation

Jack Petty and Friedrich König

SUPA School of Physics and Astronomy, University of St. Andrews, North Haugh, St. Andrews, KY16 9SS, UK

The photonic crystal fiber (PCF) is a unique medium giving us the opportunity to perform experiments in carefully chosen regimes with precision and control. Using PCFs, we can perform analogue gravity experiments to study the physics of Hawking radiation and related processes such as resonant radiation. We discuss the similarities and differences between these processes and experimentally investigate the limits of effects of this type, discovering a new regime of record efficiency. We measure a 60% energy conversion efficiency from a pump to a visible femtosecond pulse by the process of resonant radiation, and demonstrate its extraordinary tunability in wavelength and bandwidth. Beyond analogue gravity, these femtosecond visible pulses provide a desirable laser source useful across a variety of modern scientific fields.

1. Introduction

Hawking radiation [1] was suggested as the first mechanism by which black holes could emit light from the event horizon. This mechanism involves the spontaneous creation of a particle-antiparticle pair near to the event horizon with the velocity of one particle causing it to escape while the velocity of the other leads it to fall in, which can also be seen as the scattering of the quantum vacuum. To an observer at infinity, one of these particles is seen to have positive energy and the other negative, or more formally one has positive 'norm' and the other negative 'norm'. While Hawking radiation itself is strictly defined as spontaneous pair creation near the event horizon of an astrophysical black hole, it is one particular instance of a more general effect of emission into positive and negative norm partner modes which we could call the Hawking process.

In 1981, Unruh founded the field of analogue gravity [2], leading to the realisation of analogue systems in which the Hawking process could be observed.

To date, the Hawking process has been studied in a huge variety of condensed matter systems [3–7], with universality of the effect providing strong evidence for the existence of Hawking radiation. While the Hawking radiation is an extremely weak effect, when the same process is taken into an experimental laboratory we can do much to increase its detectability. Most notably we can, instead of using the vacuum state as input as in the astrophysical case, use a stimulating mode in order to increase the efficiency of pair creation in the Hawking process by many orders of magnitude.

In order to perform these experiments, the behaviour of the condensed matter systems involved must be studied intensely. In such study, it is no surprise that much interesting physics can be explored. In Section 2 of this paper, we will review the fibre-optical analogue gravity scheme [3]. In Section 3, we will present our original experimental findings from studying the mode conversion processes possible in this scheme. In Section 4, we will describe the wider implications of our findings beyond the analogue gravity context.

2. Optical Fibres for Analogue Gravity

Optics is a particularly well suited toolkit for performing analogue gravity experiments. There exist a variety of mechanisms with which an experimentalist can create optical event horizons [3,8,9]. There also exist the technologies to allow us to extract and manipulate individual emitted quanta, and the possibility to reduce the optical and thermal backgrounds to levels which allow sensitivity to the single particle, important for detecting weak effects. In addition to these experimental capabilities, there exist recent theoretical calculations to support analogue gravity in optical systems [10–16]. In this paper, we will focus on the fibre-optical scheme for analogue gravity.

(a) Nonlinearity

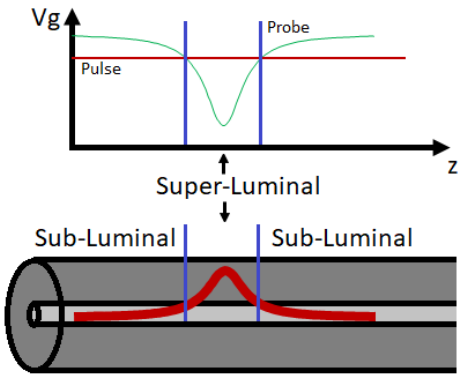

Figure 1. Cartoon of a photonic crystal fibre with the core in light grey and a propagating pulse temporal profile in red. The blue lines represent the event horizons, the border between the sub- and super-luminal regions. Above is a graph of pulse and probe group velocity explaining that a probe of carefully chosen frequency can experience both sub-luminal and super-luminal regions due to the Kerr Effect as it propagates in the fibre .

As a pulse of light propagates in a highly nonlinear photonic crystal fibre, the refractive index increases underneath the pulse due to the Kerr effect [17]. Other 'probe' waves that propagate in the same fibre experience this refractive index increase as a slowing of their speed when they are near the pulse [3]. Figure 1 shows how this effect leads to the generation of sub-luminal and super-luminal regions separated by optical event horizons (blue) which exist for certain frequencies of

probe light. This scheme gives us two event horizons in the reference frame of the pulse at which the probe speed is slowed to the pulse speed, one on the leading edge of the pulse and one on the trailing edge. It can be shown that a mode conversion process that takes place at these horizons is an analogue to the astrophysical Hawking radiation realised in a dispersive system [3].

(b) Dispersion

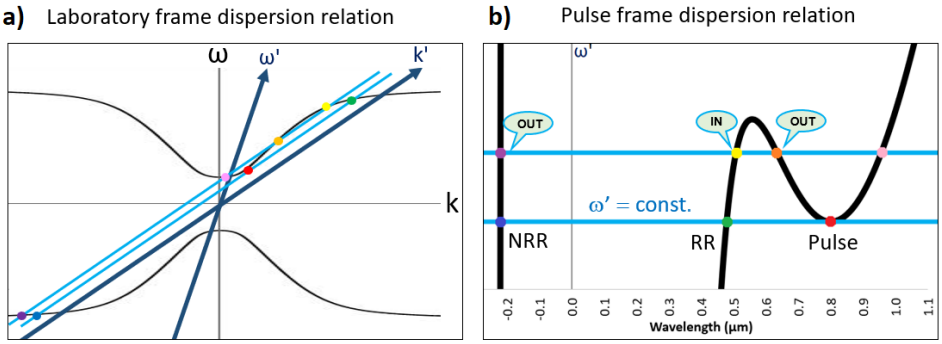

Figure 2. Dispersion relation of an example PCF in a) the laboratory frame and b) the reference frame of the pulse. The light blue lines in both plots represent constant ω'; at the pulse frequency (red, green, blue) and an external probe frequency (yellow, orange, pink, purple). Details of the dispersion relation near k=0 are neglected in a).

Of great importance to this scheme is the dispersion relation of the PCF, as this dictates the allowable modes that can propagate in the fibre. It consists of a positive branch and, symmetrically, a negative branch, represented by the black curves in Figure 2(a). A scattering process occurring in the reference frame of the pulse is governed by the conservation of frequency in this frame. Lines of constant moving frame frequency (blue in Figure 2(a)) are tilted on the laboratory frame dispersion relation and so scattering in the moving frame allows for conversion to modes with different laboratory frame frequencies. This frequency conversion at a moving scatterer is a familiar situation from the Doppler Effect. The tilting of the moving frame frequency matching condition (ω'=const.) allows for coupling to other modes on both the positive and negative branch of the dispersion relation. From a quantum fields perspective, we have modes on the positive frequency branch represented by the annihilation operator and on the negative frequency branch, now the Hermitian conjugate, represented by the creation operator. If our input is allowed to scatter to a linear combination of these positive and negative norm modes, then this process is represented by a Boguliubov transformation, giving us the creation of non-degenerate entangled photon pairs [18]. This is an example of the Hawking process, realised in an optical fibre.

(c) Resonance

If we transform Figure 2(a) by plotting the vertical axis in the reference frame of the pulse, then the ω'=const. condition becomes a horizontal line as seen in Figure 2(b). This can be seen as a resonance condition that shows which modes are available to scatter into. The horizontal axis remains in the laboratory frame, allowing us to simply find the wavelengths at which photons may be experimentally detected. In the moving frame, the pulse is at rest at the minimum of the dispersion relation due to the gradient representing the group velocity. We can see that there is one other point with gradient zero that is group velocity matched to the pulse. There are two other solutions with the same moving frequency as the pulse, as seen by the resonance condition, one called resonant radiation (RR) on the positive branch [19,20] and one called negative resonant

radiation (NRR) on the negative branch [21,22]. Given some coupling, the pulse is free to send photons to either of these solutions as long as total energy and momentum conservation are obeyed. Additionally, if we send another external input, a 'probe', labelled 'IN' in Figure 2(b), into the fibre then this too has resonant modes into which it can scatter by the ω'=const. condition, on both the positive and negative branches [3].

The positive resonant radiation has been around in the literature for decades [19,20], with experimental confirmation following the development of the photonic crystal fiber [23–25]. The detection of negative resonant radiation was much more recent [21]. This detection of NRR, in both optical fibres by the König group and in crystals by the Faccio group, was an important milestone as this was the first demonstration of coupling to negative norm modes. The scattering of probe light has also been investigated experimentally, into positive norm modes [3,26,27] and much more recently into negative norm modes [28].

3. Resonant Radiation and Hawking Radiation

(a) Interaction Length

Resonant radiation and the Hawking process differ in one important aspect that leads to vastly different experimental observations. In the case of the probe input scattering to positive and negative norm modes, the probe has a velocity mismatch to the pulse so that the probe runs into the pulse and scatters from the refractive index profile. This interaction can only exist over a finite length, depending on the relative velocity and pulse lengths. The resonant radiation process on the other hand is stimulated by the pulse photons themselves and so has an infinite interaction length. In this way, the resonant radiation case can be seen as the ideal limiting case of this type of interaction, with potentially much higher experimental efficiencies [26].

(b) Pulse Compression

In addition to this, if the pulse is launched in the anomalous dispersion regime of the optical fibre then because of the interplay of the dispersion and nonlinearity of the fibre, the pulse undergoes temporal self compression and spectral broadening [17,22]. At the input of the fibre the pulse is tens of nanometres in bandwidth but after a very short time of propagation this increases to many hundreds of nanometres and begins to overlap with the wavelength of the resonant radiation. This mode overlap or coupling between the pulse and the resonant radiation gives a huge boost to the efficiency, and this method has been used to demonstrate large energy conversion efficiencies of up to $40\,\%$ from an infra-red pulse to the visible [29–31]. This is only possible in the resonant radiation case due to the fact that the pulse self-stimulates the resonant conversion, and this same trick can not help us boost the conversion efficiency from the external probe in the Hawking process case.

(c) Efficiency

The pulse compression effect depends finely on the input parameters of the pulse; particularly the power, the wavelength, and the chirp. In our laboratory we made an experiment to see just how efficient this process could become. We sent short $50\,\mathrm{fs}$ pulses through dispersion compensation and power control into a photonic crystal fibre (NLPM760, NKT Photonics) with zero-dispersion wavelength $760\,\mathrm{nm}$, nonlinear coefficient $0.1\,\mathrm{W}^{-1}\mathrm{m}^{-1}$ and core size $1.6\,\mu\mathrm{m}$. The polarisation of the input pulses was aligned with the axis of birefringence that gave the lowest resonant radiation wavelength in this polarisation maintaining fibre. We investigated the effect of finely tuning the input parameters on the output spectrum, measured with an optical spectrum analyser sensitive from $350 - 1750\,\mathrm{nm}$. At very low powers, the output spectrum is negligibly different to the input spectrum in Figure 3(a), but as we increase the pulse energy to $0.24\,\mathrm{nJ}$ as in Figure 3(b), the nonlinearity begins to compete with the dispersion and strong spectral broadening begins to

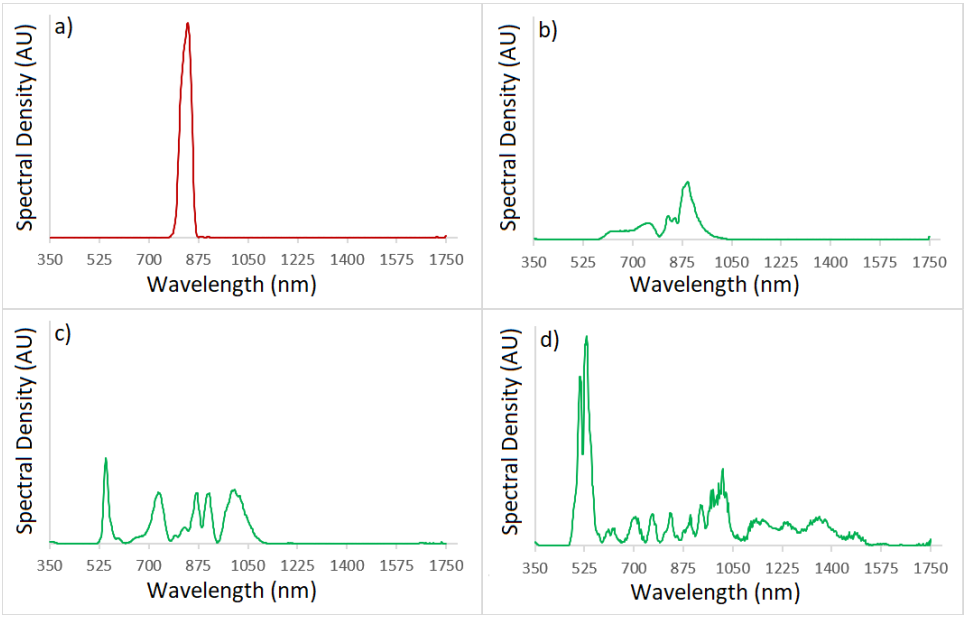

Figure 3. a) Fibre input spectrum around 830nm. b)-d) Fibre output spectra after propagating through 1.5 cm of PCF at pulse energies of b) 0.24 nJ, c) 0.48 nJ, d) 1.01 nJ. The three (green) output spectra b)-d) are normalised relative to each other, while the (red) input spectrum a) is at an arbitrary normalisation.

occur. By 0.48 nJ as in Figure 3(c), the broadening is sufficient to strongly couple the pulse to the resonant mode and large peaks start to occur at the resonant wavelength at the expense of power in the original pulse wavelengths. At input energies of 1.01 nJ the pulse has been reduced to a spectral intensity far below that of the visible peak at the fibre output, with a broadened pump remainder extending up to approximately 1500 nm. Using a thermal power meter sensitive to light up to $10\,\mu$m, the power content of the visible resonant radiation at the output of the fibre was measured as a fraction of the total fibre output power. In the best case, we have measured a record $60\,\%$ energy conversion efficiency from 830 nm input pulses to femtosecond visible pulses. By this resonant process, governed by the same mechanism as the classical (stimulated) Hawking process, energy has been extracted from the pulse so far as to destroy the analogue event horizon system, demonstrating the potential strength of these resonant effects.

4. Applications

(a) Pulse Length

Because of the high degree of pulse compression involved in the collapse of the pulse, we might expect that the resonant radiation is a femtosecond pulse itself, perhaps even shorter than the input pulse. In order to more fully characterise the visible pulses generated in this resonant radiation process, we measure the temporal length using the method of XFROG (cross-correlated frequency resolved optical gating) [32].

This method involves sending the fibre output from the resonant radiation generation along with a synchronised unchirped reference pulse into an autocorrelator as shown in Figure 4(a). In order to create the reference pulse, a fraction of the input pulse that generates the resonant radiation was taken. For this reason, the resonant radiation in this case was generated at a lower than the optimal efficiency from Section 3, using an unchirped input pulse. After the two pulses enter the autocorrelator, they are both split into two copies, one of which travels along an arm

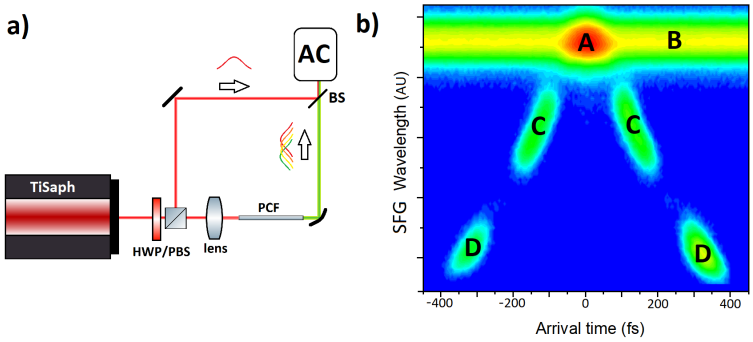

Figure 4. a) Experimental setup used for XFROG measurements. The source is a titanium-sapphire laser, with half-wave plate (HWP) and polarising beam splitter (PBS) for power control, lens to couple into PCF and beamsplitter (BS) to recombine the beams into the autocorrelator (AC). b) Output FROG trace of the whole fibre output combined with the 800 nm reference pulse, with arrival time on the horizontal axis and sum-frequency generation (SFG) wavelength on the vertical axis.

of the autocorrelator which changes its length during a scanning procedure. In this way, the reference pulse is temporally scanned across the fibre output in a sum-frequency generation crystal, producing a signal that depends on the intensity and wavelength of any fibre output present at each delay time. Because both the reference pulse and the fibre output are split into both arms of the autocorrelator, the trace has the same behaviour in both positive and negative delay, giving temporal symmetry along the delay axis when the system is correctly aligned.

The signal is displayed as a 2d plot in Figure 4(b). It contains multiple parts. Firstly, scanning the two copies of the reference pulse across each other gives an autocorrelation at label A with background at all times generated by each of the copies of the reference pulse individually at label B. At both positive and negative delay times, the cross correlation of the reference pulse with the fibre output gives peaks C and D. Peak C is from a red component generated in the non-optimal pulse collapse. Peak D is the main result of this measurement - the cross correlation of the visible resonant radiation peak with an unchirped reference pulse of known duration.

Using this method, the duration of the visible resonant radiation can be retrieved using the known duration of the reference pulse and properties of the convolution of approximately Gaussian pulses. We infer the visible peak to be as short as 39 fs, significantly shorter than the 80 fs input pulses used for this measurement.

The tilt of peaks C and D indicates that the fibre output has a small amount of chirp on it. Interestingly, the curve through C and D traces the shape of the dispersion relation of the fibre in which the resonant radiation is generated, reaffirming that the chirp on this fibre output was mainly caused by propagation through excess fibre medium. Using the fact that resonant radiation is created in an extremely small time window in an extreme pulse collapse, we can predict that resonant radiation generated very close to the end of the fibre would be smaller than 39 fs, closer to the bandwidth limited value. This potential for extremely short pulses makes resonant radiation particularly appealing as a method of generating visible laser sources [35].

(b) Tunability

As well as the high efficiency, the resonant radiation process allows for extreme wavelength tunability over the whole of the visible range by changing the input parameters of the probe and the 1.5 cm fibre. Figure 5(a) shows a variety of fibre output spectra taken with a spectrometer. This demonstrates that using input wavelengths of 800-830 nm and fibres with zero-dispersion wavelengths of 670-780 nm, the output resonant radiation peak can be tuned throughout the visible. The demonstrated >300 nm wavelength tunability, making use of several PCFs, is in

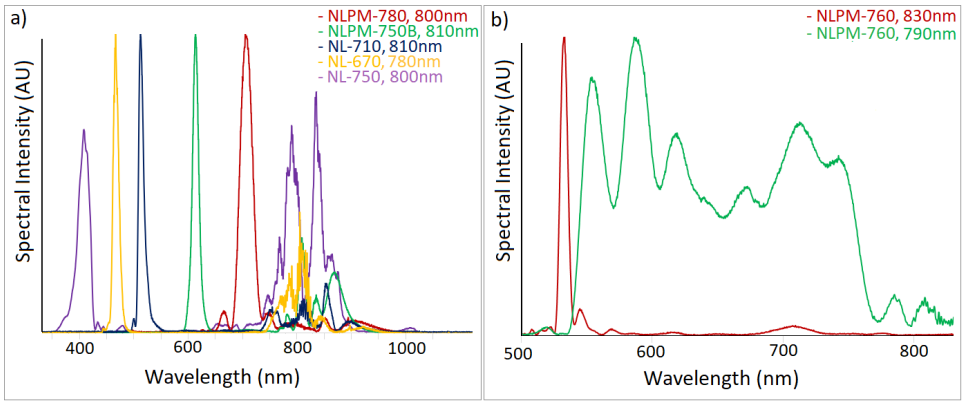

Figure 5. a) A variety of fibre output spectra showing tunability of the resonant radiation across the whole visible spectrum, normalised where possible. The narrow peaks on the left are the resonant radiation, and the other features in the infra-red are the pump remainder. b) Two fibre output spectra showing how the sensitive pulse collapse dynamics can be exploited to generate both very narrowband and very broadband outputs. In each plot, the fibre types and input wavelengths used to generate each spectra are listed.

excess of that achieved with single tapered fibres [33], while using much shorter wavelength, lower energy pulses from a Ti:Sapphire laser rather than the fiber laser used in that work. The resonant radiation wavelengths produced in these fibres is typically easier to determine experimentally than theoretically, as the fibre dispersion parameters needed for this calculation are not known with high precision. Also, the intense pulse makes a strong nonlinear modification to the dispersion relation, shifting the resonant radiation wavelength in some cases over 100 nm bluer of where the linear dispersion relation predicts.

Tunability of the output bandwidth is also possible. When the power is not much higher than at the onset of the resonant radiation effect, the visible peaks created are relatively spectrally confined to smooth, roughly Gaussian, peaks of approximately 10 nm FWHM. Larger powers usually distort and broaden the produced spectrum significantly. However, even at these larger powers it is possible to find small regions in parameter space that allow for the generation of visible peaks even more spectrally confined than those at lower powers by exploiting the violent and sensitive dynamics of the pulse collapse. Exploring small positive chirps and large powers, a similar regime to that of the highest efficiency, sharp resonant radiation peaks of down to 6 nm FWHM have been generated, as seen in Figure 5(b). The converse is similarly possible. Launching the linearly polarised pulse at an angle not precisely aligned with the axes of symmetry of the fibre causes resonant radiation to be simultaneously generated by perpendicular components of the birefringent fibre, spreading the resonant radiation spectrum. In addition, changing the input chirp and wavelength of the pulse has an important effect on the bandwidth of the resonant radiation. Combining all of these effects at our disposal, output spectra reminiscent of supercontinuum spanning many hundreds of nanometres can be generated as in Figure 5(b). This is not unprecendented given the importance of resonant radiation in supercontinuum generation in PCFs [34], although it is typically assisted by many other nonlinear processes in longer fibres than were used here. Due to the femtosecond nature of the input pulse, these extremely broadband spectra are expected to be coherent, although the input pulse energies for these extremely broadband spectra are typically < 0.5 nJ, lower than in the regime of high efficiency resonant radiation.

(c) Modern Physics Applications

These efficient and tunable femtosecond visible pulses are in high demand in fields like ultrafast microscopy, short pulse bioimaging, astrocomb generation and coherent supercontinuum generation [35]. These pulses are usually generated by frequency doubling a suitable laser source, an expensive process for which the highest reported conversion efficiency is $53\,\%$ in the femtosecond regime [36]. Remarkably, these resonant radiation experiments can take place in nothing more than 1cm of commercially available photonic crystal fibre, making the cost of the laser converter minimal. So in the quest to perform analogue gravity experiments we have inadvertently produced an important laser application.

5. Conclusion

Our journey into fibre optical analogue gravity has led to a deeper understanding of the processes responsible for realising a dispersive stimulated analogue to the astrophysical Hawking radiation. We have performed an investigation to find under which conditions conversions of this type are most efficient. This led us to investigate the low cost and robust mechanism of resonant radiation as a possible future laser source. We found an unprecedented degree of tunability in both wavelength and bandwidth and potential for extremely short and desirable femtosecond visible pulses. We also demonstrated a record $60\,\%$ energy conversion efficiency from $830\,\mathrm{nm}$ input pulses to femtosecond visible pulses. These measurements will be substantiated in future publications. It is an inevitability, with the level of understanding of our systems required to perform analogue gravity experiments, that we should make interesting discoveries along the way when we stop to enjoy the view, and this is never more true than in the rich and fruitful area of study of nonlinear fibre optics. Our work is potentially the first of many applications to come out of analogue gravity physics.

Competing Interests. The authors declare no conflicts of interest.

Funding. This work is supported by ESPRC Grant No. EP/N509759/1

Acknowledgements. We acknowledge stimulating discussions at the event 'The Next Generation of Analogue Gravity Experiments' at the Royal Society in London, December 2019.

References

1. Hawking, S. W. (1974). Black hole explosions? Nature, 248(5443), 30–31. https://doi.org/10.1038/248030a0
2. Unruh, W. G. (1981). Experimental black-hole evaporation? Physical Review Letters, 46(21), 1351–1353. https://doi.org/10.1103/PhysRevLett.46.1351
3. Philbin, T. G., Kuklewicz, C., Robertson, S., Hill, S., Konig, F., Leonhardt, U. (2007). Fiber-optical analogue of the event horizon. Science, 319(5868), 1367-1370. https://doi.org/10.1126/science.1153625
4. Rousseaux, G., Mathis, C., Maissa, P., Philbin, T. G., Leonhardt, U. (2008). Observation of negative-frequency waves in a water tank: A classical analogue to the Hawking effect? New Journal of Physics, 10(5). https://doi.org/10.1088/1367-2630/10/5/053015
5. Weinfurtner, S., Tedford, E. W., Penrice, M. C. J., Unruh, W. G., Lawrence, G. A. (2011). Measurement of stimulated hawking emission in an analogue system. Physical Review Letters, 106(2). https://doi.org/10.1103/PhysRevLett.106.021302
6. Nguyen, H. S., Gerace, D., Carusotto, I., Sanvitto, D., Galopin, E., Lemaître, A., Sagnes, I., Bloch, J., Amo, A. (2015). Acoustic black hole in a stationary hydrodynamic flow of microcavity polaritons. Physical Review Letters, 114(3). https://doi.org/10.1103/PhysRevLett.114.036402
7. Steinhauer, J. (2016). Observation of quantum Hawking radiation and its entanglement in an analogue black hole. Nature Physics, 12(10), 959–965. https://doi.org/10.1038/nphys3863
8. Belgiorno, F., Cacciatori, S. L., Clerici, M., Gorini, V., Ortenzi, G., Rizzi, L., Rubino, E., Sala, V. G., Faccio, D. (2010). Hawking radiation from ultrashort laser pulse filaments. Physical Review Letters, 105(20). https://doi.org/10.1103/PhysRevLett.105.203901

9. Elazar, M., Fleurov, V., Bar-Ad, S. (2012). All-optical event horizon in an optical analog of a Laval nozzle. Physical Review A - Atomic, Molecular, and Optical Physics, 86(6). https://doi.org/10.1103/PhysRevA.86.063821
10. Finazzi, S., Carusotto, I. (2012). Quantum vacuum emission in a nonlinear optical medium illuminated by a strong laser pulse. Physical Review A, 87(2). https://doi.org/10.1103/PhysRevA.87.023803
11. Leonhardt, U., Robertson, S. (2012). Analytical theory of Hawking radiation in dispersive media. New Journal of Physics, 14(5). https://doi.org/10.1088/1367-2630/14/5/053003
12. Robertson, S., Leonhardt, U. (2014). Integral method for the calculation of Hawking radiation in dispersive media. I. Symmetric asymptotics. Physical Review E - Statistical, Nonlinear, and Soft Matter Physics, 90(5). https://doi.org/10.1103/PhysRevE.90.053302
13. Belgiorno, F., Cacciatori, S. L., Dalla Piazza, F. (2015). Hawking effect in dielectric media and the Hopfield model. Physical Review D - Particles, Fields, Gravitation and Cosmology, 91(12). https://doi.org/10.1103/PhysRevD.91.124063
14. Jacquet, M., König, F. (2015). Quantum vacuum emission from a refractive-index front. Physical Review A - Atomic, Molecular, and Optical Physics, 92(2). https://doi.org/10.1103/PhysRevA.92.023851
15. Linder, M. F., Schützhold, R., Unruh, W. G. (2016). Derivation of Hawking radiation in dispersive dielectric media. Physical Review D, 93(10). https://doi.org/10.1103/PhysRevD.93.104010
16. Jacquet, M. J., Koenig, F. (2019). Analytical description of quantum emission in optical analogues to gravity. Retrieved from http://arxiv.org/abs/1908.02060
17. Agrawal, G. (2013). Nonlinear Fiber Optics-Fifth Edition. (Elsevier BV) https://doi.org/10.1016/B978-0-12-397023-7.00010-3
18. Bogoljubov, N. N. (1958). On a new method in the theory of superconductivity. Il Nuovo Cimento Series 10, 7(6), 794–805. https://doi.org/10.1007/BF02745585
19. Wai, P. K. A., Menyuk, C. R., Lee, Y. C., and Chen, H. H. (1986). Nonlinear pulse propagation in the neighborhood of the zero-dispersion wavelength of monomode optical fibers. Optics Letters 11, 464-466. https://doi.org/10.1364/OL.11.000464
20. Akhmediev, N., Karlsson, M. (1995). Cherenkov radiation emitted by solitons in optical fibers. Physical Review A, 51(3), 2602–2607. https://doi.org/10.1103/PhysRevA.51.2602
21. Rubino, E., McLenaghan, J., Kehr, S. C., Belgiorno, F., Townsend, D., Rohr, S., Kuklewicz, C. E., Leonhardt, U., König, F., Faccio, D. (2012). Negative-frequency resonant radiation. Physical Review Letters, 108(25). https://doi.org/10.1103/PhysRevLett.108.253901
22. McLenaghan, J., König, F. (2014). Few-cycle fiber pulse compression and evolution of negative resonant radiation. New Journal of Physics, 16(6). https://doi.org/10.1088/1367-2630/16/6/063017
23. Tartara, L., Cristiani, I., Degiorgio, V. (2003). Blue light and infrared continuum generation by soliton fission in a microstructured fiber. Applied Physics B: Lasers and Optics, 77(2–3), 307–311. https://doi.org/10.1007/s00340-003-1172-0
24. Cristiani, I., Tediosi, R., Tartara, L. and Degiorgio, V. (2004). Dispersive wave generation by solitons in microstructured optical fibers. Optics Express 12, 124-135. https://doi.org/10.1364/OPEX.12.000124
25. Tu, H. and Boppart, S. A. (2009) Optical frequency up-conversion by supercontinuum-free widely-tunable fiber-optic Cherenkov radiation. Optics Express 17, 9858-9872 (2009) https://doi.org/10.1364/OE.17.009858
26. Choudhary, A., König, F. (2012). Efficient frequency shifting of dispersive waves at solitons. Optics Express, 20(5), 5538. https://doi.org/10.1364/oe.20.005538
27. Tartara, L. (2015). Soliton control by a weak dispersive pulse. Journal of the Optical Society of America B, 32(3), 395. https://doi.org/10.1364/josab.32.000395
28. Drori, J., Rosenberg, Y., Bermudez, D., Silberberg, Y., Leonhardt, U. (2019). Observation of Stimulated Hawking Radiation in an Optical Analogue. Physical Review Letters, 122(1). https://doi.org/10.1103/PhysRevLett.122.010404
29. Chang, G., Chen, L.-J., Kärtner, F. X. (2010). Highly efficient Cherenkov radiation in photonic crystal fibers for broadband visible wavelength generation. Optics Letters, 35(14), 2361. https://doi.org/10.1364/ol.35.002361
30. Zhang, X. Ben, Zhu, X., Chen, L., Jiang, F. G., Yang, X. B., Peng, J. G., Li, J. Y. (2013). Enhanced violet Cherenkov radiation generation in GeO2-doped photonic crystal fiber. Applied Physics B: Lasers and Optics, 111(2), 273–277. https://doi.org/10.1007/s00340-012-5329-6

31. Chan, M.-C., Lien, C.-H., Lu, J.-Y., Lyu, B.-H. (2014). High power NIR fiber-optic femtosecond Cherenkov radiation and its application on nonlinear light microscopy. Optics Express, 22(8), 9498. https://doi.org/10.1364/oe.22.009498
32. Linden, S., Giessen, H., Kuhl, J. (1998). XFROG ? A New Method for Amplitude and Phase Characterization of Weak Ultrashort Pulses. Physica Status Solidi (B), 206(1), 119–124. https://doi.org/10.1109/CLEO.1998.676502
33. Liu, X., Laegsgaard, J., Iegorov, R., Svane, A., Ilday, F., Tu, H., Boppart, S., Turchinovich, D. (2017). Nonlinearity-tailored fiber laser technology for low-noise, ultra-wideband tunable femtosecond light generation. Photonics Research 5, 750-761. https://doi.org/10.1364/PRJ.5.000750
34. Dudley, J. M., Genty, G., and Coen, S. (2006). Supercontinuum generation in photonic crystal fiber. Reviews of Modern Physics, 78, 1135-1184. https://doi.org/10.1103/RevModPhys.78.1135
35. Liu, X., Svane, A. S., Lægsgaard, J., Tu, H., Boppart, S. A., Turchinovich, D. (2015). Progress in Cherenkov femtosecond fiber lasers. Journal of Physics D: Applied Physics, 49(2). https://doi.org/10.1088/0022-3727/49/2/023001
36. Kanseri, B., Bouillard, M., Tualle-Brouri, R. (2016). Efficient frequency doubling of femtosecond pulses with BIBO in an external synchronized cavity. Optics Communications, 380, 148–153. https://doi.org/10.1016/j.optcom.2016.05.067